

# A Nonreciprocal Multi-channel Bandstop Filter Using the Generalized Fibonacci Multiferroic Superlattices with the Silver-mean Sequence

Zhenghua Tang<sup>1</sup>, Xuhui Liu<sup>2, \*</sup>, Dajun Lei<sup>1</sup>, Jianquan Huang<sup>1</sup>,  
Feng Qiu<sup>1</sup>, Haiming Deng<sup>1</sup>, Chunzhi Jiang<sup>1</sup>, and Min Yao<sup>1</sup>

**Abstract**—The generalized Fibonacci multiferroic superlattices (GFMS) are composed of single-phase multiferroic domains with simultaneous polarization and magnetization and are defined by the binary substitutional rule ( $B \rightarrow B^m A, A \rightarrow B, m = 2, 3$ ). We propose to construct a nonreciprocal multi-channel bandstop filter by the GFMS. The couplings between electromagnetic waves and lattice vibration of multiferroic material with ferroelectric and ferromagnetic (or antiferromagnetic) orders can be invoked either through piezoelectric or piezomagnetic effects and can lead to the creation of polaritonic band structure. The plane wave expansion method with first-order approximation predicts the existence of multiple band gaps, and electromagnetic waves lying within the band gaps are prohibited, and the band gaps with respect to forward electromagnetic waves (FEWs) and backward electromagnetic waves (BEWs) are asymmetric. The forbidden band structures with FEWs and BEWs are calculated by the transfer matrix method and multiple frequency channels with unidirectional transmission of electromagnetic waves can be further confirmed. Nine and twenty transmission dips in transmission spectra for the BEWs in the frequency range of  $\bar{\omega} = 0.4\text{--}0.6$  (17.06 GHz–25.59 GHz) are found in the GFMS with  $m = 2$  and 3, respectively, in which the BEWs are prohibited while the FEWs can travel. Thus, the GFMS has all the conditions for the nonreciprocal multi-channel bandstop filter. Besides, the GFMS can also be applied to construct compact multi-channel one-way electromagnetic waveguides.

## 1. INTRODUCTION

The nonreciprocal bandstop filter as a great potential application of microwave device has attracted great attention during the past two decades, in which the properties for the FEWs and the BEWs are not consistent. A variety of nonreciprocal microwave devices [1–6] have been investigated which involve filters with a turnstile open gyromagnetic resonator [2], bidirectional erbium-doped fiber [3], an optically coherent high birefringence fiber transversal filter structure [4], magnetostatic surface wave [6], and involve an fiber Fabry-Perot resonator [1], as well as an orthogonal frequency division multiplexing system [5]. Generally, the asymmetry for FEWs and BEWs originates from time-reversal and space inversion symmetries (TRSIS) breaking due to magnetic materials integrated into the devices.

Multiferroic materials with the TRSIS breaking as the coexistence of magnetic and electric parameters can be regarded as a potential candidate for the nonreciprocal bandstop filter. A general single-phase multiferroic material is one that two or three distinct properties [7], such as ferroelectricity, ferromagnetism and ferroelasticity, coexisting in the same phase, in which magnetic and electric order parameters are included. The multiferroic materials also usually allow for the coexistence

---

Received 9 November 2015, Accepted 7 December 2015, Scheduled 18 December 2015

\* Corresponding author: Xuhui Liu (mfliu2005@163.com).

<sup>1</sup> Xiangnan University-Gospel Joint laboratory of Microwave Communication Technology, Xiangnan University, Chenzhou 423000, China. <sup>2</sup> College of Science, Hunan University of Science and Engineering, Yongzhou 425199, China.

of piezoelectricity and piezomagnetism [8]. The electric field to these materials can induce lattice strain because of piezoelectric effect and the magnetic field to them can induce the lattice strain via piezomagnetic effect as well. Furthermore, the electric and magnetic fields can couple to the lattice vibration simultaneously, which has a contribution to the magnetoelectric effect. One of application approaches [9] on the multiferroic materials is constructed as superlattices with simultaneous electric polarization and magnetization in order to manipulate electromagnetic waves.

Up to now, many investigations on superlattices have been carried out, which include the dielectric [10,11] properties and periodical structures with one-way electromagnetic propagation modes [12–17]. However, there are almost no attentions on the generalized Fibonacci multiferroic superlattices (GFMS) with silver-mean sequence, especially as the nonreciprocal compact multi-channel bandstop filter or the multi-channel one-way waveguide. In this paper, we consider the GFMS with fourth-order silver-mean sequence illustrated in Figure 1. It has a spontaneous magnetization along  $z$ -axis direction and a spontaneous polarization along  $y$ -axis direction in the same domain. The positively and negatively domains with thickness  $L_{\pm}$  are the two building blocks  $A$  and  $B$ . They have been arranged repeatedly along one direction according to the substitution rules of generalized Fibonacci sequence described by successive application ( $B \rightarrow B^m A$  and  $A \rightarrow B$ ,  $m = 2, 3$ ) [18], with the zeroth generation  $s_0 = A$ ,  $s_1 = B$ , and  $s_2 = B^m A$ . Consider an electromagnetic wave impinging on the GFMS, the coupling between the acoustic wave originating from the lattice vibration and electromagnetic waves can occur, which lead to the creation of the coupled polaritonic band structure. The band structures with respect to the FEWs and BEWs are asymmetric due to the TRSIS breaking originating from coexisting of the electric and magnetic order parameters simultaneously in the GFMS.

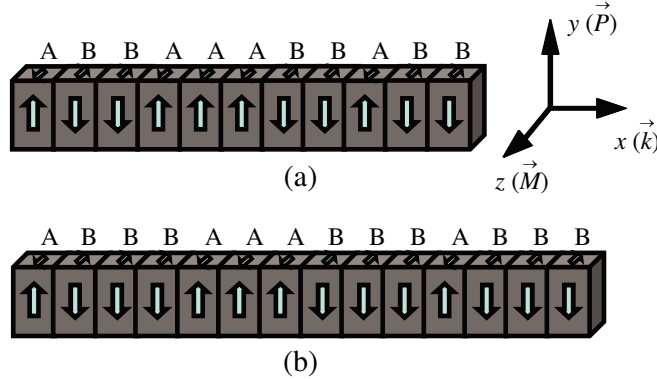


**Figure 1.** A schematic diagram of quasi-one-dimensional generalized Fibonacci multiferroic superlattices with the generation of  $l = 4$  and the substitution index (a)  $m = 2$  and (b)  $m = 3$ . Lattice displacement  $u_x$  and wavevector  $k$  are along  $x$ -axis, the magnetic field  $H_z$  and magnetization  $M_z$  are along  $\pm z$ -axis, the electric field  $E_y$  and polarization  $P_y$  are along  $\pm y$ -axis.

This work presents a design that the nonreciprocal compact multi-channel bandstop filter or the multi-channel one-way waveguide can be constructed on the basis of the GFMS. The plane wave expansion method with first-order approximation indicates there are many band gaps in the GFMS, and the band gaps with respect to the FEWs and BEWs are asymmetric. Transmission dips for the BEWs can be observed in transmission spectra while for the FEWs do not appear in the same frequency as the former.

## 2. GOVERNING EQUATIONS

The GFMS is composed of the domains with the coexistence of polarization and magnetization. The purpose of the experimental construction is to achieve the couplings between the electric and magnetic components of an electromagnetic wave and lattice vibration simultaneously. As a consequence, the experimental setting must ensure the piezomagnetic and piezoelectric effects can occur simultaneously. There are many different arrangements for the domains according to the orientations of polarization

and magnetization for the GFMS. An arrangement of domains with  $+\vec{P}$ ,  $+\vec{M}$  and  $-\vec{P}$ ,  $-\vec{M}$  has been considered, where  $\pm\vec{P}$  represent the polarization along positive and negative  $y$  axis, and  $\pm\vec{M}$  denote the magnetization along positive and negative  $z$  axis are considered in our paper. The lattice constant of  $l$ th generation sequence is  $a_l = F_l^1 L_+ + F_l^2 L_-$ , where  $F_l^1$  and  $F_l^2$  is the number of positive and negative domains. Figure 1 shows that the electric field  $E_y(x, t)$ , the magnetic field  $H_z(x, t)$  and the lattice displacement  $u_x(x, t)$  are in the  $y$ ,  $z$  and  $x$  axis, respectively. The dynamic properties of the system are described by the coupled equation set as follows:

$$\begin{aligned} \left(\frac{\omega L}{2\pi c_s}\right) \bar{E}_y(\bar{x}, \omega) &= -i\alpha_1 \frac{\partial}{\partial \bar{x}} \bar{H}_z(\bar{x}, \omega) - \beta_1 \left(\frac{\omega L}{2\pi c_s}\right) \theta_1(\bar{x}) \frac{\partial}{\partial \bar{x}} \bar{u}_x(\bar{x}, \omega) \\ &\quad - \gamma_1 \theta_1(x) \theta_2(x) \left(\frac{\omega L}{2\pi c_s}\right) \bar{H}_z(\bar{x}, \omega), \end{aligned} \quad (1)$$

$$\begin{aligned} \left(\frac{\omega L}{2\pi c_s}\right) \bar{H}_z(\bar{x}, \omega) &= -i\alpha_2 \frac{\partial}{\partial \bar{x}} \bar{E}_y(\bar{x}, \omega) - \beta_2 \left(\frac{\omega L}{2\pi c_s}\right) \theta_2(\bar{x}) \frac{\partial}{\partial \bar{x}} \bar{u}_x(\bar{x}, \omega) \\ &\quad - \gamma_2 \theta_1(x) \theta_2(x) \left(\frac{\omega L}{2\pi c_s}\right) \bar{E}_y(\bar{x}, \omega), \end{aligned} \quad (2)$$

$$\left(\frac{\omega L}{2\pi c_s}\right)^2 \bar{u}_x(\bar{x}, \omega) = -\frac{\partial^2}{\partial \bar{x}^2} \bar{u}_x(\bar{x}, \omega) + \frac{\partial}{\partial \bar{x}} [\theta_1(\bar{x}) \bar{E}_y(\bar{x}, \omega)] + \frac{\partial}{\partial \bar{x}} [\theta_2(\bar{x}) \bar{H}_z(\bar{x}, \omega)]. \quad (3)$$

Where  $\bar{E}_y(\bar{x}, \omega)$ ,  $\bar{H}_z(\bar{x}, \omega)$  and  $\bar{u}_x(\bar{x}, \omega)$  correspond to the Fourier transformed quantities of  $E_y(x, t)$ ,  $H_z(x, t)$  and  $u_x(x, t)$ , respectively. The above equation set is written in dimensionless form. The dimensionless variables  $x = \bar{x}L/2\pi$ ,  $u_x(x, t) = \bar{u}_x(\bar{x}, t)/2\pi$ ,  $\bar{H}_z(x, t) = |\bar{T}_{31}|H_z(x, t)$  and  $\bar{E}_y(x, t) = |\bar{d}_{21}|E_y(x, t)$  are introduced.  $\theta_1(\bar{x}) = \pm 1$  denote the domains with magnetization along positive and negative  $z$  axis,  $\theta_2(\bar{x}) = \pm 1$  denote the domains along positive and negative  $y$  axis, respectively.  $c_s = 1/\sqrt{\rho \bar{s}_{11}}$  is the sound velocity of the media. The six dimensionless material parameters are  $\alpha_1 = |\bar{T}_{31}|/\mu_0 \bar{\mu} |\bar{d}_{21}| c_s$ ,  $\alpha_2 = |\bar{d}_{21}|/\epsilon_0 \bar{\epsilon} |\bar{T}_{31}| c_s$ ,  $\beta_2 = k_{11} |\bar{d}_{21}|^2 / \epsilon_0 \bar{\epsilon}$ ,  $\beta_1 = k_{11} |\bar{T}_{31}|^2 / \mu_0 \bar{\mu}$ ,  $\gamma_1 = \bar{\alpha}_{23} |\bar{T}_{31}| / \mu_0 \bar{\mu} |\bar{d}_{21}|$  and  $\gamma_2 = \bar{\alpha}_{23} |\bar{d}_{21}| / \epsilon_0 \bar{\epsilon} |\bar{T}_{31}|$ .  $\beta_1$  and  $\beta_2$  denote the magneto-mechanical transducer and electromechanic coefficients and describe the coupling strength between the electric and magnetic field components of electromagnetic waves and lattice vibration, respectively.  $\gamma_1$  and  $\gamma_2$  denote the electro-magnetic and magneto-electric coefficients that describe the energy transfer efficiency between the electric and magnetic energy. Where  $\bar{\epsilon} = \epsilon_{22} - \Delta\epsilon_{22}$  is the effective dielectric constant.  $\bar{\mu} = \mu_{33} - \Delta\mu_{33}$  and  $\bar{\alpha}_{23}(x) = \alpha_{23}(x) - \Delta\alpha_{23}(x)$  correspond to effective permeability and magnetoelectric coefficient, respectively.

$$\Delta\epsilon_{22} = \frac{1}{\epsilon_0} [d_{21}(x)k_{11}\bar{d}_{21}(x) + d_{22}(x)k_{21}\bar{d}_{22}(x) + d_{23}(x)k_{23}\bar{d}_{23}] \quad (4)$$

$$\Delta\mu_{33} = \frac{1}{\mu_0} [T_{31}(x)k_{11}\bar{T}_{31}(x) + T_{32}(x)k_{21}\bar{T}_{32}(x) + T_{33}(x)k_{33}\bar{T}_{33}(x)] \quad (5)$$

$$\Delta\alpha_{23}(x) = [T_{31}(x)k_{11}\bar{d}_{21}(x) + T_{32}(x)k_{21}\bar{d}_{22}(x) + T_{33}(x)k_{31}\bar{d}_{33}(x)]. \quad (6)$$

The reduced bulk modulus  $k_{ij}$  is defined as the inverse matrix of elastic compliance tensor and the reduced piezoelectric coefficients  $\bar{d}_{21}(x)$ ,  $\bar{d}_{22}(x)$  and  $\bar{d}_{23}(x)$ , and the piezomagnetic coefficients  $\bar{T}_{31}(x)$ ,  $\bar{T}_{32}(x)$  and  $\bar{T}_{33}(x)$  have the following forms:

$$\bar{d}_{21}(x) = d_{21}(x) + d_{22}(x) \frac{k_{12}}{k_{11}} + d_{23}(x) \frac{k_{13}}{k_{11}}, \quad \bar{d}_{22}(x) = d_{21}(x) + d_{22}(x) \frac{k_{22}}{k_{21}} + d_{23}(x) \frac{k_{23}}{k_{21}}, \quad (7)$$

$$\bar{d}_{23}(x) = d_{21}(x) + d_{22}(x) \frac{k_{32}}{k_{31}} + d_{23}(x) \frac{k_{33}}{k_{31}}, \quad \bar{T}_{31}(x) = T_{31}(x) + T_{32}(x) \frac{k_{12}}{k_{11}} + T_{33}(x) \frac{k_{13}}{k_{11}}, \quad (8)$$

$$\bar{T}_{32}(x) = T_{31}(x) + T_{32}(x) \frac{k_{22}}{k_{21}} + T_{33}(x) \frac{k_{23}}{k_{21}}, \quad \bar{T}_{33}(x) = T_{31}(x) + T_{32}(x) \frac{k_{32}}{k_{31}} + T_{33}(x) \frac{k_{33}}{k_{31}}. \quad (9)$$

An ideal interface between the positive and negative domains is assumed. The transverse electric and magnetic fields, the longitudinal displacement and the stress component across the domain interface are continuous. The transfer matrices  $M(\bar{L}_i, \bar{\omega})$  can describe the basic properties of different

domains and are given in Ref. [14]. The whole matrix of the GFMS can be obtained by multiplying multiferroic domain matrices according to the corresponding sequences. We extend the plane wave method describing the pure piezoelectric Thue-Morse superlattices in Ref. [18] to the system of the GFMS, in which  $\bar{E}_y(\bar{x}, \bar{\omega})$ ,  $\bar{H}_z(\bar{x}, \bar{\omega})$ ,  $\bar{u}_x(\bar{x}, \bar{\omega})$  can be expanded in the reciprocal space in the following:  $\bar{E}_y(\bar{x}, \bar{\omega}) = \sum_{k_{n_l}} G(\bar{k} + k_{n_l}, \bar{\omega}) \exp[i(\bar{k} + k_{n_l})\bar{x}]$ ,  $\bar{H}_z(\bar{x}, \bar{\omega}) = \sum_{k_{n_l}} H(\bar{k} + k_{n_l}, \bar{\omega}) \exp[i(\bar{k} + k_{n_l})\bar{x}]$ ,  $\bar{u}_x(\bar{x}, \bar{\omega}) = \sum_{k_{n_l}} (-i)U(\bar{k} + k_{n_l}, \bar{\omega}) \exp[i(\bar{k} + k_{n_l})\bar{x}]$ ,  $k_{n_l}$  denotes the reciprocal lattice vector with  $l$ th-order Fibonacci sequence with  $n_l$  representing an integer.

$$\begin{aligned} \bar{\omega}G(\bar{k} + k_{n_l}, \bar{\omega}) &= -\alpha_1(\bar{k} + k_{n_l})H(\bar{k} + k_{n_l}, \bar{\omega}) - \beta_1\bar{\omega} \sum_{k_{m_l}} (\bar{k} + k_{m_l})\theta_1(k_{n_l} - k_{m_l})U(\bar{k} + k_{m_l}, \bar{\omega}) \\ &\quad - \gamma_1\theta_1(k_{n_l} - k_{m_l})\theta_2(k_{n_l} - k_{m_l})\bar{\omega}H(\bar{k} + k_{n_l}, \bar{\omega}) \end{aligned} \quad (10)$$

$$\begin{aligned} \bar{\omega}H(\bar{k} + k_{n_l}, \bar{\omega}) &= -\alpha_2(\bar{k} + k_{n_l})G(\bar{k} + k_{n_l}, \bar{\omega}) - \beta_2\bar{\omega} \sum_{k_{m_l}} (\bar{k} + k_{m_l})\theta_2(k_{n_l} - k_{m_l})U(\bar{k} + k_{m_l}, \bar{\omega}) \\ &\quad - \gamma_2\theta_1(k_{n_l} - k_{m_l})\theta_2(k_{n_l} - k_{m_l})\bar{\omega}G(\bar{k} + k_{n_l}, \bar{\omega}) \end{aligned} \quad (11)$$

$$\begin{aligned} \bar{\omega}^2U(\bar{k} + k_{n_l}, \bar{\omega}) &= (\bar{k} + k_{n_l})^2U(\bar{k} + k_{n_l}, \bar{\omega}) - (\bar{k} + k_{n_l}) \sum_{k_{m_l}} \theta_1(k_{n_l} - k_{m_l})G(\bar{k} + k_{n_l}, \bar{\omega}) \\ &\quad - (\bar{k} + k_{n_l}) \sum_{k_{m_l}} \theta_2(k_{n_l} - k_{m_l})H(\bar{k} + k_{n_l}, \bar{\omega}). \end{aligned} \quad (12)$$

Since  $\beta_1 \ll \alpha_1$  and  $\beta_2 \ll \alpha_2$ , and the electromagnetic wave-lattice vibration coupling take places near the center of the Brillouin zone, in the framework of first-order perturbation theory, the coupled modes mainly include the folded phonon branches with wavenumber  $\bar{k} + k_{m_l}$  and the unfolded photon branch with wave number  $\bar{k}$ . Thus the Eqs. (10)–(12) can be transformed as follows:

$$\bar{\omega}G(\bar{k}, \bar{\omega}) = -\alpha_1\bar{k}H(\bar{k}, \bar{\omega}) - \beta_1\bar{\omega}(\bar{k} + k_{m_l})\theta_1(-m_l)U(\bar{k} + k_{m_l}, \bar{\omega}) - \gamma_1\theta_1(m_l)\theta_2(m_l)\bar{\omega}H(\bar{k}, \bar{\omega}), \quad (13)$$

$$\bar{\omega}H(\bar{k}, \bar{\omega}) = -\alpha_2\bar{k}G(\bar{k}, \bar{\omega}) - \beta_2\bar{\omega}(\bar{k} + k_{m_l})\theta_2(-m_l)U(\bar{k} + k_{m_l}, \bar{\omega}) - \gamma_2\theta_1(m_l)\theta_2(m_l)\bar{\omega}G(\bar{k}, \bar{\omega}), \quad (14)$$

$$\bar{\omega}^2U(\bar{k} + k_{m_l}, \bar{\omega}) = (\bar{k} + k_{m_l})^2U(\bar{k} + k_{m_l}, \bar{\omega}) - (\bar{k} + k_{m_l})\theta_1(m_l)G(\bar{k}, \bar{\omega}) - (\bar{k} + k_{m_l})\theta_2(m_l)H(\bar{k}, \bar{\omega}). \quad (15)$$

$\theta_i(m_l)$  ( $i = 1, 2$ ) denotes the Fourier component of  $\theta_i(\bar{x})$ . Eliminating the independent variables of magnetic field  $H(\bar{k}, \bar{\omega})$  and lattice displacement  $U(\bar{k} + k_{m_l}, \bar{\omega})$ , the above Eqs. (13)–(15) can be transformed into the equation for electric field. Four different eigensolutions for a homogeneous multiferroic domain can be obtained at a given frequency, which consist of two pairs of traveling wave, one pair is along the forward direction of the domain, the other pair is along the backward direction. The eigensolutions  $\bar{\omega}_{\pm i}$  ( $i = 1, 2$ ) are written in the following,

$$\bar{\omega}_{+1}, \bar{\omega}_{+2} = \frac{1}{2} \left( \sqrt{\delta - \frac{2\delta_1}{3}} \pm \sqrt{-\delta - \frac{4\delta_1}{3} - \frac{2\delta_2}{\sqrt{\delta - 2\delta_1/3}}} \right) - \frac{(\alpha_1\gamma_2 + \alpha_2\gamma_1)\theta_1(m_l)\theta_2(m_l)\bar{k}}{4(1 - \gamma_1\gamma_2\theta_1^2(m_l)\theta_2^2(m_l))}, \quad (16)$$

$$\bar{\omega}_{-1}, \bar{\omega}_{-2} = \frac{1}{2} \left( -\sqrt{\delta - \frac{2\delta_1}{3}} \pm \sqrt{-\delta - \frac{4\delta_1}{3} + \frac{2\delta_2}{\sqrt{\delta - 2\delta_1/3}}} \right) - \frac{(\alpha_1\gamma_2 + \alpha_2\gamma_1)\theta_1(m_l)\theta_2(m_l)\bar{k}}{4(1 - \gamma_1\gamma_2\theta_1^2(m_l)\theta_2^2(m_l))}. \quad (17)$$

The forward and backward propagating modes are marked by subindex  $\pm$ .  $\delta_i$ s indicate the coefficients of polynomial equation of third degree determined by the material parameters

$$\begin{aligned} \delta_1 &= -\frac{3}{8} \left( \frac{(\alpha_1\gamma_2 + \alpha_2\gamma_1)\theta_1(m_l)\theta_2(m_l)\bar{k}}{1 - \gamma_1\gamma_2\theta_1^2(m_l)\theta_2^2(m_l)} \right)^2 + \frac{1}{1 - \gamma_1\gamma_2\theta_1^2(m_l)\theta_2^2(m_l)} ((\gamma_1\beta_2\theta_1^2(m_l)|\theta_2(m_l)|^2 \\ &\quad + \gamma_2\beta_1\theta_2^2(m_l)|\theta_1(m_l)|^2 - \beta_1|\theta_1(m_l)|^2 - \beta_2|\theta_2(m_l)|^2 \\ &\quad + \gamma_1\gamma_2\theta_1^2(m_l)\theta_2^2(m_l) - 1)(\bar{k} + k_{m_l})^2 - \alpha_1\alpha_2\bar{k}^2), \end{aligned} \quad (18)$$

$$\begin{aligned}
\delta_2 = & -\frac{1}{8} \left( \frac{(\alpha_1\gamma_2 + \alpha_2\gamma_1)\theta_1(m_l)\theta_2(m_l)\bar{k}}{1 - \gamma_1\gamma_2\theta_1^2(m_l)\theta_2^2(m_l)} \right)^3 + \frac{1}{2(1 - \gamma_1\gamma_2\theta_1^2(m_l)\theta_2^2(m_l))^2} ((\alpha_1\gamma_2 + \alpha_2\gamma_1)\theta_1(m_l)\theta_2(m_l)\bar{k}) \\
& ((\gamma_1\beta_2\theta_1^2(m_l)|\theta_2(m_l)|^2 + \gamma_2\beta_1\theta_2^2(m_l)|\theta_1(m_l)|^2 - \beta_1|\theta_1(m_l)|^2 - \beta_2|\theta_2(m_l)|^2 + \gamma_1\gamma_2\theta_1^2(m_l)\theta_2^2(m_l) - 1) \\
& (\bar{k} + k_{m_l})^2 - \alpha_1\alpha_2\bar{k}^2) + \frac{\bar{k}(\bar{k} + k_{m_l})^2}{1 - \gamma_1\gamma_2\theta_1^2(m_l)\theta_2^2(m_l)} (\alpha_1\beta_2\theta_1(m_l)\theta_2(-m_l) + \alpha_2\beta_1\theta_1(-m_l)\theta_2(m_l) \\
& + (\alpha_1\gamma_2 + \alpha_2\gamma_1)\theta_1(m_l)\theta_2(m_l)), \tag{19}
\end{aligned}$$

$$\begin{aligned}
\delta_3 = & -\frac{3}{256} \left( \frac{(\alpha_1\gamma_2 + \alpha_2\gamma_1)\theta_1(m_l)\theta_2(m_l)\bar{k}}{1 - \gamma_1\gamma_2\theta_1^2(m_l)\theta_2^2(m_l)} \right)^4 + \frac{1}{16(1 - \gamma_1\gamma_2\theta_1^2(m_l)\theta_2^2(m_l))^3} ((\alpha_1\gamma_2 + \alpha_2\gamma_1) \\
& \theta_1(m_l)\theta_2(m_l)\bar{k})^2 (\gamma_1\beta_2\theta_1^2(m_l)|\theta_2(m_l)|^2 + \gamma_2\beta_1\theta_2^2(m_l)|\theta_1(m_l)|^2 - \beta_1|\theta_1(m_l)|^2 \\
& - \beta_2|\theta_2(m_l)|^2 + \gamma_1\gamma_2\theta_1^2(m_l)\theta_2^2(m_l) - 1) (\bar{k} + k_{m_l})^2 - \alpha_1\alpha_2\bar{k}^2) + \frac{\bar{k}(\bar{k} + k_{m_l})^2}{4(1 - \gamma_1\gamma_2\theta_1^2(m_l)\theta_2^2(m_l))^2} \\
& (\alpha_1\gamma_2 + \alpha_2\gamma_1)\theta_1(m_l)\theta_2(m_l)\bar{k}(\alpha_1\beta_2\theta_1(m_l)\theta_2(-m_l)) + \alpha_2\beta_1\theta_1(-m_l)\theta_2(m_l) \\
& + (\alpha_1\gamma_2 + \alpha_2\gamma_1)\theta_1(m_l)\theta_2(m_l)) + \frac{\alpha_1\alpha_2\bar{k}^2(\bar{k} + k_{m_l})^2}{1 - \gamma_1\gamma_2\theta_1^2(m_l)\theta_2^2(m_l)}, \tag{20}
\end{aligned}$$

and  $\delta$  is a real special solution of the polynomial equation

$$\begin{aligned}
\delta = & \sqrt[3]{\left(\frac{1}{27}\delta_1^3 - \frac{4}{3}\delta_1\delta_3 + \frac{\delta_2^2}{2}\right) + \sqrt{\left(\frac{1}{27}\delta_1^3 - \frac{4}{3}\delta_1\delta_3 + \frac{\delta_2^2}{2}\right)^2 - \left(\frac{\delta_1^2}{9} + \frac{4\delta_3^2}{3}\right)^3}} \\
& + \sqrt[3]{\left(\frac{1}{27}\delta_1^3 - \frac{4}{3}\delta_1\delta_3 + \frac{\delta_2^2}{2}\right) - \sqrt{\left(\frac{1}{27}\delta_1^3 - \frac{4}{3}\delta_1\delta_3 + \frac{\delta_2^2}{2}\right)^2 - \left(\frac{\delta_1^2}{9} + \frac{4\delta_3^2}{3}\right)^3}}. \tag{21}
\end{aligned}$$

Here,  $\pm 1$  denote the electromagnetic propagating modes while  $\pm 2$  refer to the acoustic propagating modes. Although the dispersion relations in purely piezoelectric or piezomagnetic materials are polarization direction independent and are symmetrical with respect to the forward and backward directions, the coexistence of electric polarization and magnetization in the GFMS breaks the time-reversal and space inversion symmetries and the dispersion relations  $\bar{\omega}_{+1} \neq \bar{\omega}_{-1}$  and  $\bar{\omega}_{+2} \neq \bar{\omega}_{-2}$  can be obtained. The coupled polaritonic band gap for the forward direction is determined by  $\Delta\bar{\omega}_+ = \bar{\omega}_{+2} - \bar{\omega}_{+1}$  and for the backward direction is determined by  $\Delta\bar{\omega}_- = \bar{\omega}_{-2} - \bar{\omega}_{-1}$ . The band gap difference  $\Delta\bar{\omega} = \Delta\bar{\omega}_+ - \Delta\bar{\omega}_-$  for the forward and backward directions can give the frequency window allowing one-way propagating electromagnetic modes. The position of  $\Delta\bar{\omega}_\pm$  is determined by the nonvanishing Fourier components  $\theta_i(m_l)$ , and the bandwidth of  $\Delta\bar{\omega}$  is dominated by the six dimensionless coefficients derived from the actual material parameters in the right hand of Eqs. (10)–(12).

### 3. NUMERICAL RESULTS AND DISCUSSION

The dimensionless parameters used in Eqs. (1)–(3) are  $\alpha_1 = 1.11 \times 10^7$ ,  $\alpha_2 = 29.2$ ,  $\beta_1 = 0.170$ ,  $\beta_2 = 4.47 \times 10^{-7}$ ,  $\gamma_1 = 1.27$ , and  $\gamma_2 = 3.33 \times 10^{-6}$ . The electromechanic coefficient is quite robust. The bandgap as an important research object has been concerned since it can show clearly the frequency ranges that photons do not propagate. The coupled polaritonic forbidden band structures with respect to the forward and backward electromagnetic waves for the GFMS with  $m = 2, 3$  are calculated by the transfer matrix and originate from a two-step process: (1) the periodical modulation of electric polarization and magnetization in multiferroic domains causes the phonon dispersion branch to be folded, which can provide the possibility for the coupling between the only photon branch and phonon branches; (2) the whole matrix  $M_l(\bar{L}_i, \bar{\omega})$  for the  $l$ -th generation GFMS with  $m = 2, 3$  can be obtained by successively multiplying the matrices with the prescribed sequences. Its purely imaginary eigenvalues are extracted. The corresponding frequency ranges for them are given, which represent the forbidden propagation modes, and the photons do not propagate in those frequency ranges.

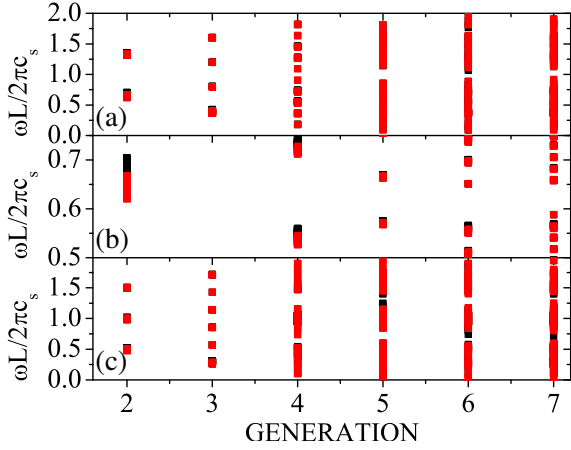


**Figure 2.** The evolutionary relationship of polaritonic band gaps with the Fibonacci generation  $l = 2 \sim 7$  and  $\bar{L}_{M+} = \bar{L}_{M-} = \pi$  in frequency range of (a)  $\bar{\omega} = 0\text{--}2.0$ , (b)  $\bar{\omega} = 0.50\text{--}0.75$  for the GFMS with  $m = 2$  and (c)  $\bar{\omega} = 0\text{--}2.0$  for the GFMS with  $m = 3$ . The red solid squares denote the forbidden gaps for the backward electromagnetic waves, and the black solid squares represent the forbidden gaps for the forward electromagnetic waves.

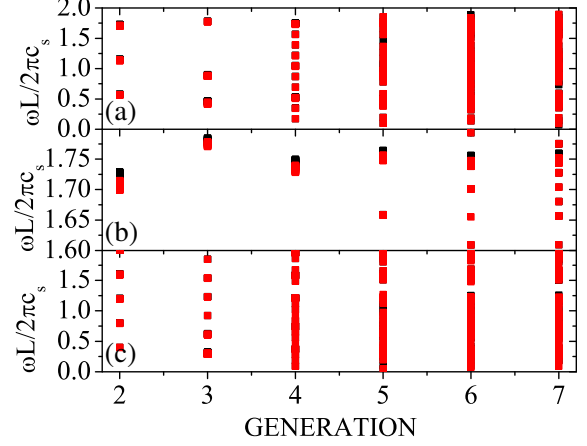


**Figure 3.** The evolutionary relationship of polaritonic band gaps with the Fibonacci generation  $l = 2 \sim 7$ ,  $\bar{L}_{M+} = 0.5\pi$  and  $\bar{L}_{M-} = 1.5\pi$  in frequency range of (a)  $\bar{\omega} = 0\text{--}2.0$ , (b)  $\bar{\omega} = 1.60\text{--}1.80$  for the GFMS with  $m = 2$  and (c)  $\bar{\omega} = 0\text{--}1.99$  for the GFMS with  $m = 3$ . The other parameters are the same as Figure 2.

The forbidden band structures for the GFMS with  $m = 2, 3$  are calculated and illustrated in Figures 2(a)–(c) with  $\bar{L}_+ = \bar{L}_- = \pi$ , respectively. The horizontal axis represents the generation  $l$  and the vertical axis denotes the reduced frequency. The red solid squares denote the band gaps for the BEWs, and the black solid squares represent the band gaps for the FEWs. We can find easily that the red solid squares and the black solid squares are not completely coincident. As shown in Figure 2(a), the band gap differences with regard to the FEWs and BEWs for the GFMS with  $m = 2$  can be found in the vicinity of  $\bar{\omega} = 0.6$  and  $\bar{\omega} = 1.3$ . In order to observe the band gap differences more clearly, the band structure around  $\bar{\omega} = 0.65$  is enlarged and replotted in Figure 2(b), where an obvious band gap difference can be observed around  $\bar{\omega} = 0.67$  and can provide a frequency window allowing electromagnetic waves propagating only along a single direction. The reason for the existence of the band gap differences is the TRSIS breaking in the GFMS due to the coexistence of electric polarization and magnetization in multiferroic domains.

Besides, the forbidden band structures are also the relative domain sizes in a unit cell dependent and for the GFMS with  $m = 2, 3$  are shown in Figures 3(a)–(c) with  $\bar{L}_+ = 0.5\pi$  and  $\bar{L}_- = 1.5\pi$ . The band gap differences with respect to the FEWs and BEWs can be observed in the neighborhood of  $\bar{\omega} = 0.6$ ,  $\bar{\omega} = 1.1$  and  $\bar{\omega} = 1.7$  for the GFMS with  $m = 2$  in Figure 3(a) and in the neighborhood of  $\bar{\omega} = 0.4$ ,  $\bar{\omega} = 0.8$ ,  $\bar{\omega} = 1.2$ ,  $\bar{\omega} = 1.6$  and  $\bar{\omega} = 2.0$  for the the GFMS with  $m = 3$  in Figure 3(c), respectively, which show the number of frequency channels having one-way electromagnetic propagation modes increasing compared with the corresponding results in Figure 2.

Although the presence of the band gaps with respect to the FEWs and BEWs has been confirmed by the forbidden band structures shown in Figure 3, the values of the absolute or relative bandwidth (gap-to-midfrequency ratio) for them still can not be calculated quantitatively. To achieve this purpose, the thickness of multiferroic domains are chosen as  $L_{M+} = L_{M-} = 0.5\ \mu\text{m}$ , and transmission spectra are calculated and illustrated in Figure 4. The horizontal axis represents the reduced frequency and the vertical axis denotes the normalized transmission coefficient. The black square line denotes the transmission curve for the FEW while the red uptriangle line represents that of the BEW. The black square and the red uptriangle lines are not completely coincident, and multiple transmission dips can be observed around  $\bar{\omega} = 0.5$  (21.3 GHz),  $\bar{\omega} = 0.7$  (29.82 GHz) and  $\bar{\omega} = 1.5$  (63.9 GHz) as shown in

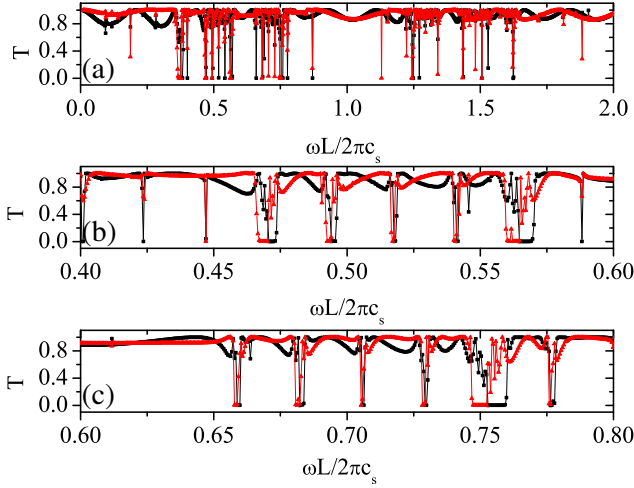


**Figure 4.** The transmission spectrum of the multiferroic Fibonacci superlattices with  $m = 2$  ( $S_{23}$ ) as a function of reduced frequency  $\bar{\omega}$  with  $L_{M+} = L_{M-} = \pi$ . (a) For frequency range of  $\bar{\omega} = 0-2.0$ . (b) For frequency range of  $\bar{\omega} = 0.4-0.6$ . (c) For frequency range of  $\bar{\omega} = 0.6-0.8$ . The black square line denotes the transmission curve for the forward electromagnetic wave while the red uptriangle line represents that of the backward electromagnetic wave.

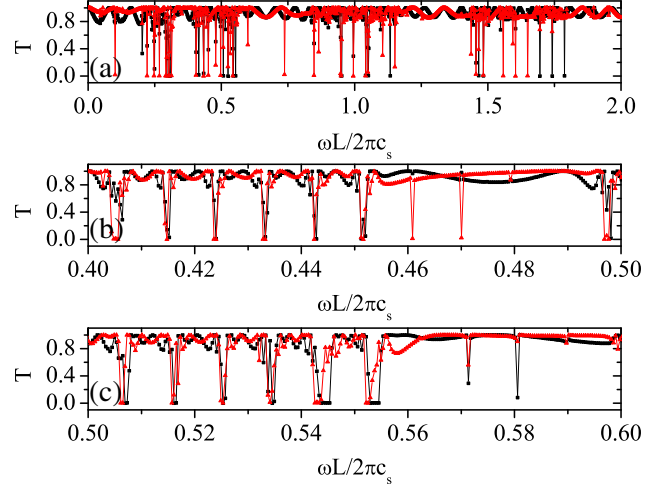


**Figure 5.** The transmission spectrum of the multiferroic Fibonacci superlattices with  $m = 3$  ( $S_{23}$ ) as a function of reduced frequency  $\bar{\omega}$  with  $L_{M+} = L_{M-} = \pi$ . (a) For frequency range of  $\bar{\omega} = 0-2.0$ . (b) For frequency range of  $\bar{\omega} = 0.4-0.5$ . (c) For frequency range of  $\bar{\omega} = 0.5-0.6$ .

Figure 4(a). In order to observe the band gaps more clearly, the transmission spectra around  $\bar{\omega} = 0.5$  (21.3 GHz) and  $\bar{\omega} = 0.7$  (29.82 GHz) are enlarged and replotted in Figures 4(b) and 4(c).

The transmission dips for the BEWs can be observed around  $\bar{\omega} = 0.468$  (19.96 GHz),  $\bar{\omega} = 0.493$  (21.02 GHz),  $\bar{\omega} = 0.517$  (22.05 GHz),  $\bar{\omega} = 0.540$  (23.03 GHz) and  $\bar{\omega} = 0.562$  (23.97 GHz), and the corresponding relative (absolute) bandwidths for them are 0.77% (0.154 GHz), 0.40% (0.084 GHz), 0.21% (0.046 GHz), 0.24% (0.055 GHz) and 0.9% (0.215 GHz), respectively. Moreover, there are still three additional transmission dips with narrow frequency ranges beside them. Six transmission dips for the BEWs in the frequency ranges of  $\bar{\omega} = 0.6-0.8$  can also be found in Figure 4(c), in which the FEWs can propagate while the BEWs are prohibited. Similarly, the transmission dips in the black square curves in Figures 4(a)–(c) denote the band gaps for the FEWs, where the FEWs can not pass through the GFMS, but the BEWs is allowed to pass. In addition, the transmission spectrum of the GFMS is also the binary substitutional index  $m$  dependent.

As in the situation in Figure 5(a), the transmission dips are more intensive than the corresponding results shown in Figure 4(a) when the substitution index  $m$  is changed from 2 to 3. Nine transmission dips can also be observed at  $\bar{\omega} = 0.4-0.5$  and are shown in Figure 5(b). The distribution relationship in frequency axis of transmission dips shown in Figure 5(c) is very similar to that of the results illustrated in Figure 5(b). Thus, the GFMS with  $m = 2$  and 3 demonstrate multi-channel band gaps or multi-channel one-way electromagnetic transmission and can be constructed nonreciprocal compact multi-channel bandstop filters or multi-channel one-way electromagnetic waveguides.

#### 4. CONCLUSION

In this paper, a program on a nonreciprocal multi-channel bandstop filter using the GFMS has been proposed. We have predicted the existence of multiple band gaps and unidirectional frequency channels in the GFMS with substitution indices  $m = 2$  and 3 by the plane wave expansion method in the framework of first-order perturbation theory. The forbidden structures and transmission spectra are

utilized to verify and calculate the relative (absolute) bandwidths of those channels quantitatively, and there are nine transmission dips for BEWs in the frequency range of  $\bar{\omega} = 0.4\text{--}0.6$  for the GFMS with  $m = 2$ , in which the FEWs can pass while the BEWs are prohibited. Thus the multi-channel bandstop filter is nonreciprocal with regard to the FEWs and BEWs. The GFMS can be potentially useful for multiple channel unidirectional waveguides or isolators. In addition, the decrease of symmetry in a unit cell and the increase of substitution index  $m$  in the GFMS can also lead to increasing the number of unidirectional transmission channels of electromagnetic waves.

## ACKNOWLEDGMENT

This work was supported by General Project Hunan Provincial Education Office [13C886], [13C881] and [14C1060], and Program for Science and Technology Innovative Research Team in Higher Educational Institutions of Hunan Province and Project of Science and Technology in Chenzhou City.

## REFERENCES

1. Jopson, R. M., J. Stone, L. W. Stulz, and S. J. Licht, "Nonreciprocal transmission in a fiber Fabry-Perot resonator containing a magneto-optic material," *IEEE Photonic Techn. Lett.*, Vol. 2, No. 10, 702–704, 1990.
2. Heszajn, J., C. S. Cheng, and B. A. Wilcock, "A nonreciprocal tunable waveguide directional filter using a turnstile open gyromagnetic resonator," *IEEE Trans. Microw. Theory Techn.*, Vol. 41, No. 11, 1950–1958, 1993.
3. Oh, T. W., J. H. Shin, H. D. Kim, C. H. Lee, M. S. Lee, and B. Y. Kim, "Bidirectional Erbium-doped fibre amplifier with non-reciprocal optical filter," *Electron. Lett.*, Vol. 37, No. 5, 283–284, 2001.
4. Lai, Y. C., W. Zhang, J. A. R. Williams, and I. Bennion, "Bidirectional nonreciprocal wavelength-interleaving coherent fiber transversal filter," *IEEE Photonic Tech. Lett.*, Vol. 16, No. 2, 500–502, 2004.
5. Lli, A. T., M. Codreanu, and M. Juntti, "Compensation of non-reciprocal interference in adaptive MIMO-OFDM cellular systems," *IEEE Trans. Wire. Commun.*, Vol. 6, No. 2, 545–555, 2007.
6. Wu, J., X. Yang, S. Beguhn, J. Lou, and N. X. Sun, "Nonreciprocal tunable low-loss bandpass filters with ultra-wideband isolation based on magnetostatic surface wave," *IEEE Trans. Microw. Theory Techn.*, Vol. 60, No. 12, 3959–3968, 2012.
7. Schmid, H., "Multiferroic magnetoelectrics," *Ferroelectrics*, Vol. 162, 317–338, 1994.
8. Lee, J. H., L. Fang, E. Vlahos, X. L. Ke, Y. W. Jung, L. F. Kourkoutis, J. W. Kim, P. J. Ryan, T. Heeg, M. Roeckerath, V. Goian, M. Bernhagen, R. Uecker, P. C. Hammel, K. M. Rabe, S. Kamba, J. Schubert, J. W. Freeland, D. A. Muller, C. J. Fennie, P. Schiffer, V. Gopalan, E. J. Halperin, and D. G. Schlom, "A strong ferroelectric ferromagnet created by means of spin-lattice coupling," *Nature*, Vol. 466, 954–958, 2010.
9. Tang, Z. H. and W. Y. Zhang, "Nonreciprocal multiferroic superlattices with broken parity symmetry," *Int. J. Mod. Phys. B*, Vol. 26, 1250021, 2012.
10. Negro, L. D., M. Stolfi, Y. Yi, J. Michel, X. Duan, L. C. Kimerling, J. LeBlanc, and J. Haavisto, "Photon band gap properties and omnidirectional reflectance in Si/SiO<sub>2</sub> Thue-Morse quasicrystals," *Appl. Phys. Lett.*, Vol. 84, 5186, 2004.
11. Jiang, X., Y. Zhang, S. Feng, K. C. Huang, Y. Yi, and J. D. Joannopoulos, "Photonic band gaps and localization in the Thue-Morse structures," *Appl. Phys. Lett.*, Vol. 86, 201110, 2005.
12. Figotin, A. and I. Vitebskiy, "Electromagnetic unidirectionality in magnetic photonic crystals," *Phys. Rev. B*, Vol. 67, 165210, 2003.
13. Haldane, F. D. M. and S. Raghu, "Possible realization of directional optical waveguides in photonic crystals with Broken Time-Reversal symmetry," *Phys. Rev. Lett.*, Vol. 100, 013904, 2008.
14. Takeda, H. and S. John, "Compact optical one-way waveguide isolators for photonic-band-gap microchips," *Phys. Rev. A*, Vol. 78, 203804, 2008.

15. Yu, Z. F., G. Veronis, Z. Wang, and S. H. Fan, "One-way electromagnetic waveguide formed at the interface between a plasmonic metal under a static magnetic field and a photonic crystal," *Phys. Rev. Lett.*, Vol. 100, 023902, 2008.
16. Wang, Z., Y. D. Chong, J. D. Joannopoulos, and M. Soljačić, "Reflection-free one-way edge modes in a gyromagnetic photonic crystal," *Phys. Rev. Lett.*, Vol. 100, 013905, 2008.
17. Yablonovitch, E., "One-way road for light," *Nature*, Vol. 461, 744, 2009.
18. Liu, Z. X. and W. Y. Zhang, "Bifurcation in band-gap structures and extended states of piezoelectric Thue-Morse superlattices," *Phys. Rev. B*, Vol. 75, 064207, 2007.